*Manuscript

Formation of chondrules in a moderately high dust enriched disk: evidence from oxygen isotopes of chondrules from the Kaba CV3 chondrite

Andreas T. Hertwig*, Céline Defouilloy, and Noriko T. Kita

WiscSIMS, Department of Geoscience, University of Wisconsin-Madison, Madison, WI 53706, USA.

November 17, 2017

Revision, submitted to Geochimica et Cosmochimica Acta

*Corresponding author: hertwig@wisc.edu

ABSTRACT

Oxygen three-isotope analysis by secondary ion mass spectrometry of chondrule olivine and pyroxene in combination with electron microprobe analysis were carried out to investigate 24 FeO-poor (type I) and 2 FeO-rich (type II) chondrules from the Kaba (CV) chondrite. The Mg#'s of olivine and pyroxene in individual chondrules are uniform, which confirms that Kaba is one of the least thermally metamorphosed CV3 chondrites. The majority of chondrules in Kaba contain olivine and pyroxene that show indistinguishable $\Delta^{17}O$ values (= $\delta^{17}O - 0.52 \times \delta^{18}O$) within analytical uncertainties, as revealed by multiple spot analyses of individual chondrules. One third of chondrules contain olivine relict grains that are either ^{16}O-rich or ^{16}O-poor relative to other indistinguishable olivine and/or pyroxene analyses in the same chondrules. Excluding those isotopically recognized relicts, the mean oxygen isotope ratios ($\delta^{18}O$, $\delta^{17}O$, and $\Delta^{17}O$) of individual chondrules are calculated, which are interpreted to represent those of the final chondrule melt. Most of these isotope ratios plot on or slightly below the primitive chondrule mineral (PCM) line on the oxygen three-isotope diagram, except for the pyroxene-rich type II chondrule that plots above the PCM and on the terrestrial fractionation line. The $\Delta^{17}O$ values of type I chondrules range from ~ –8‰ to ~ –4‰; the pyroxene-rich type II chondrule yields ~0‰, the olivine-rich type II chondrule ~ –2‰. In contrast to the ungrouped carbonaceous chondrite Acfer 094, the Yamato 81020 CO3, and the Allende CV3 chondrite, type I chondrules in Kaba only possess $\Delta^{17}O$ values below –3‰ and a pronounced bimodal distribution of $\Delta^{17}O$ values, as evident for those other chondrites, was not observed for Kaba.

Investigation of the Mg#-$\Delta^{17}O$ relationship revealed that $\Delta^{17}O$ values tend to increase with decreasing Mg#'s, similar to those observed for CR chondrites though data from Kaba cluster at the high Mg# (>98) and the low $\Delta^{17}O$ end (–6‰ and –4‰). A mass balance model

involving ^{16}O-rich anhydrous dust ($\Delta^{17}O$ = –8‰) and ^{16}O-poor water ice ($\Delta^{17}O$ = +2‰) in the chondrule precursors suggests that type I chondrules in Kaba would have formed in a moderately high dust enriched protoplanetary disk at relatively dry conditions (~50-100× dust enrichment compared to Solar abundance gas and less than 0.6× ice enhancement relative to CI chondritic dust). The olivine-rich type II chondrule probably formed in a disk with higher dust enrichment (~2000× Solar).

1. INTRODUCTION

Chondrules - a main constituent of most chondritic meteorites - are spherical, melted objects that formed by transient high-temperature events in the proto-planetary disk (e.g., Hewins, 1996; Rubin, 2000; Connolly and Desch, 2004; Ciesla, 2005; Morris et al., 2012). Since the recognition of isotopic anomalies in the Allende CV chondrite in the early 1970s (Clayton et al., 1973, 1977), numerous oxygen isotope studies on primitive carbonaceous chondrites have targeted the variabilities among bulk meteorites, as well as those of CAIs and chondrules (e.g, Clayton, 1993; Clayton and Mayeda, 1999; Jones et al., 2004; Krot et al., 2006; Yurimoto et al., 2008, and references therein). In general, oxygen isotope ratios of chondrules in carbonaceous chondrites plot in the oxygen three-isotope diagram below the terrestrial fractionation (TF) line and along a slope ~1 line, for instance parallel to the CCAM (carbonaceous chondrite anhydrous minerals) line, while those in ordinary chondrites cluster slightly above the TF line (e.g., Clayton 1993).

By using secondary ion mass spectrometers (SIMS), high precision (sub-‰) mineral-scale isotope data of chondrule minerals have become increasingly available in recent years (e.g., Chaussidon et al., 2008; Kita et al., 2010; Connolly and Huss, 2010; Rudraswami et al., 2011; Ushikubo et al., 2012; Schrader et al., 2013, 2014, 2017; Tenner et al., 2013, 2015; Nagashima et al., 2015). In contrast to bulk analyses, in-situ measurements of primary chondrule minerals, such as olivine, low-Ca pyroxene and mesostasis phases allow for an evaluation of the isotopic homogeneity of single chondrules. A growing number of studies have established that most chondrules are internally homogeneous in terms of their $\Delta^{17}O$ (= $\delta^{17}O - 0.52 \times \delta^{18}O$) values except for minor occurrence of relict olivine grains (e.g., Kita et al., 2010; Rudraswami et al., 2011; Tenner et al., 2013, 2015, 2017; Schrader et al., 2017). In particular, according to the analyses of ungrouped carbonaceous chondrite Acfer 094, in which both thermal metamorphism and aqueous alteration in the parent body was minimal, Ushikubo et al. (2012) clearly demonstrated that oxygen isotope ratios of olivine and pyroxene phenocrysts are indistinguishable from those of glassy mesostasis. Presuming that this is the general case, i.e., chondrule phenocrysts and mesostasis have indistinguishable $\Delta^{17}O$ values at the time of chondrule formation, it is now possible to deduce the composition of the isotopically homogenized melt by measuring chondrule phenocrysts in other chondrites even if oxygen isotope ratios of glassy mesostasis were altered due to parent body processes (e.g., in Semarkona LL3 by Kita et al., 2010).

It has been suggested that chondrules formed in an open system with respect to major oxides, such as MgO and SiO_2, which evaporated and re-condensed during melting (e.g., Tissandier et al., 2002; Alexander, 2004; Nagahara et al., 2008). Under a dust-enriched environment (e.g., Ebel and Grossman, 2000), the ambient gas present during chondrule formation would have oxygen isotope ratios similar to those of average solid precursors, since oxygen in the ambient gas would predominately originate from these precursors (e.g., Ushikubo et al., 2012). Further, Ushikubo et al. (2012) suggested that the internally homogeneous oxygen isotope ratios within a single chondrule were the result of isotope exchange between ambient gas and chondrule melt that occurred rapidly due to evaporation and re-condensation of major oxides from the chondrule melt.

The Mg#'s of chondrules, defined as the molar MgO/(MgO+FeO) % of mafic chondrule minerals, mainly depend on the redox conditions during chondrule-formation (Ebel and Grossman, 2000). Oxygen fugacities required to form FeO-poor (type I) or FeO-rich (type II) chondrules in carbonaceous chondrites (log fO_2: up to iron-wüstite buffer for type II; IW – 6 to –

2 for type I chondrules; e.g., Ebel and Grossmann, 2000; Tenner et al., 2015) are higher than estimates for the Solar nebula (log fO_2: ~ IW – 6 at 1600K; e.g., Krot et al., 2000). The more oxidizing redox conditions were likely imposed by enhancement (relative to Solar abundances) of dust particles and H_2O ice (e.g., Ebel and Grossman, 2000; Fedkin and Grossman, 2006, 2016; Schrader et al., 2013; Tenner et al., 2015). In carbonaceous chondrites, many studies have found type I chondrules to be generally ^{16}O-rich compared to type II chondrules (e.g., Kunihiro et al., 2004, 2005; Connolly and Huss, 2010; Schrader et al., 2013). Further, Ushikubo et al. (2012) and Tenner et al. (2013) observed a bimodal distribution of Δ^{17}O values that is related to Mg#'s of chondrules in Acfer 094 and Y-81020 (CO3), respectively. The majority of chondrules possess Δ^{17}O values of ~ –5‰ and Mg#>97; other chondrules show Δ^{17}O values of ~ –2‰ and a wide range of Mg# (100-40). In CB and CH chondrites, the majority of chondrules are type I with Δ^{17}O values of ~ –2‰ (Krot et al., 2010), while type II chondrules have Δ^{17}O values of ~ +1.5‰ (Nakashima et al., 2010). In the case of CR chondrites, the majority of chondrules are type I showing a larger range of Δ^{17}O values from –6‰ to –1‰, while minor type II chondrules span from –2‰ to 0‰ (e.g., Connolly and Huss, 2010; Schrader et al., 2013, 2014, 2017; Tenner et al., 2015).

The overall tendency of higher chondrule Δ^{17}O values in combination with lower Mg#'s across carbonaceous chondrites suggests the existence of ^{16}O-poor water ice among chondrule precursors in carbonaceous chondrite forming regions (e.g., Connolly and Huss, 2010; Ushikubo et al., 2012; Schrader et al., 2013). By detailed examination of Mg#'s and corresponding Δ^{17}O values among type I chondrules in CR chondrites, Tenner et al. (2015) observed a monotonic increase in Δ^{17}O values with decreasing Mg#, which was never observed in other chondrite groups before. Tenner et al. (2015) uses an oxygen isotope mass balance model in combination with expressions that link dust enrichment and abundance of water ice to the fO_2 of the chondrule melt in order to explain $\Delta^{17}O$ values and Mg#'s of chondrules. By applying $\Delta^{17}O$ values of –6‰ and +5‰ for anhydrous dust and water ice, respectively, the model estimated that type I chondrules in CR formed under 100-200× dust-enrichments relative to solar composition gas with variable amounts of water ice from 0 to 0.8× the nominal water ice content of CI chondritic dust. Tenner et al. (2015) stated that CR chondrites, Acfer 094, CO, and perhaps CV chondrites all contain chondrules with high Mg#'s (>98) and $\Delta^{17}O$ values ranging from –6‰ to –4‰. This range of compositions was also found to be the dominant chondrule type in the Y-82094 ungrouped carbonaceous chondrite (Tenner et al., 2017).

The literature data about the Mg#-$\Delta^{17}O$ relationship for chondrules from CV chondrites, as summarized in Tenner et al. (2015), requires re-examination because of the following reasons. Earlier SIMS studies are mostly not at sub-‰ precision level and mainly include olivine analyses and only a limited amount of low-Ca pyroxene analyses (e.g., Choi et al., 2000; Jones et al., 2004; Libourel and Chaussidon, 2011), hence, rendering it difficult to evaluate the mineral-scale isotopic homogeneity of these chondrules. Chaussidon et al. (2008) measured oxygen isotope ratios of several chondrule constituents in Vigarano CV3 and, for a somewhat limited number of chondrules, in the Mokoia and Efremovka CV3 chondrites; however, corresponding information about the mineral chemistry, especially the Mg#'s for each individual chondrule, were not provided. Conversely, a complete data set of oxygen isotope ratios of chondrule phases, including olivine, low-Ca pyroxene, and, where applicable, spinel and plagioclase was published by Rudraswami et al. (2011) for Allende, but the evaluation of the Mg#-$\Delta^{17}O$ relationship is made difficult by significant thermal metamorphism experienced by this chondrite (e.g., Krot et al., 1995; Bonal et al., 2006). Since diffusion of Mg and Fe in olivine and pyroxene is considerably faster than diffusion of oxygen (Dohmen and Chakraborty, 2007; Farver, 2010), chondrules more likely preserve primary oxygen isotopic compositions than Mg#'s when subjected to thermal metamorphism. For example, even though many olivine grains show higher FeO contents (lower Mg#'s) than coexisting low-Ca pyroxenes in chondrules of the Allende CV3, most chondrules are still homogeneous in oxygen isotope ratios at analytical precisions (Rudraswami et al., 2011).

Here we present SIMS oxygen three-isotope analysis of chondrules from Kaba in order to understand the chondrule formation environment and oxygen isotope reservoirs for the CV chondrite-forming region. Kaba is one of the least thermally metamorphosed CV3 chondrites (Kimura and Ikeda, 1998; Krot et al., 1998; Grossman and Brearley, 2005; Bonal et al., 2006, Busemann et al., 2007) and a member of the Bali-like oxidized subgroup (McSween, 1977). In particular, representative dust-enrichment and ice-enhancement factors of the local disk region are evaluated using the oxygen isotope mass balance model of Tenner et al. (2015) by applying model parameters suitable for the CV chondrule-forming region. Unlike Allende, chondrules in Kaba likely preserve primary Mg#'s in addition to $\Delta^{17}O$ values that are representative for conditions during chondrule formation, an assumption tested by comparing Mg# of olivine and pyroxene within each chondrule.

2. ANALYTICAL TECHNIQUES

2.1. Electron microscopy

One thin section of Kaba (USNM 1052-1) was imaged (BSE, SE) and the petrography of chondrules investigated with a Hitachi S-3400N scanning electron microscope (SEM). The chemical composition of olivine and pyroxene grains were determined by a Cameca SX-51 electron microprobe (20nA, 15keV, fully focused beam); plagioclase and high-Ca pyroxene of the mesostasis were analyzed by a Cameca SXFive (10nA, 15keV, 10μm beam). The SEM and both electron microprobes are hosted at the Department of Geoscience at UW-Madison. On both electron microprobes, concentrations of the oxides SiO_2, TiO_2, Al_2O_3, Cr_2O_3, MgO, FeO, MnO, CaO, K_2O, and Na_2O were acquired and counting times on the peak and background were set to 10s and 5s, respectively. The 3σ detection limits (wt%) for these oxides (in the order mentioned above) were at most: 0.05, 0.06, 0.04, 0.07, 0.05, 0.07, 0.07, 0.04, 0.03, and 0.06, respectively. Data reduction, including ZAF/φ(ρz) corrections, was done with the “Probe for EPMA” software suite (Donovan, 2015). The following standards were used for olivine and pyroxene analyses (on Cameca SX-51): Ti: rutile, Al: jadeite, Cr: synthetic Cr_2O_3, Fe: synthetic hematite, Mn: manganese olivine, Ca: wollastonite, K: microcline, Na: jadeite, and depending on mineral type and composition: Si: synthetic enstatite, synthetic forsterite, Fo_{83}, manganese olivine; Mg: synthetic enstatite, synthetic forsterite, Fo_{83}, amphibole. Analyses of plagioclase and high-Ca pyroxene in the chondrule mesostasis were performed on a Cameca SXFive, using the same suite of standards except for the following elements: Si: synthetic enstatite, An_{78}, An_{67}; Al: jadeite, An_{95}; Fe: fayalite; Ca: An_{78}, An_{95}; Na: jadeite, albite, An_{78}.

2.2. SIMS oxygen isotope analyses

The in-situ oxygen three-isotope analysis of olivine and pyroxene was carried out during two separate sessions with the Cameca IMS 1280 SIMS at the UW-Madison using multi-collector Faraday cups and following analytical protocols similar to those of Kita et al. (2010) and Tenner et al. (2013). In both sessions, Cs^+ primary ion intensity was set to ~3 nA in order to generate a secondary $^{16}O^-$ intensity of ~3×10^9 cps (counts per second). During the first session, the primary beam was tuned to form an ellipsoid-shaped spot of 14×10 μm, similar to the condition used in previous studies (e.g, Tenner et al., 2015, 2017). In the second session, the primary beam aperture was enlarged (>200 μm, normally 100-150 μm) and resulted in a diffused beam shape (Gaussian beam in both sessions). Consequently, we reduced the beam size to ~10 μm but rastered 5 × 5 μm over the sample surface to produce a roundish spot of 12 μm diameter. The intensity of $^{16}O^{1}H^{-}$ was monitored automatically at the end of each analysis by using a X-deflector between sector magnet and detectors in order to correct the contribution from tailing of the $^{16}O^{1}H^{-}$ peak to the $^{17}O^{-}$ signal. The correction was always insignificant (≤0.1‰).

Typically, 12-18 analyses of unknowns were bracketed by 8 analyses (4 before and 4 after unknowns) of the San Carlos olivine standard ($\delta^{18}O$ = 5.32‰ VSMOW, Kita et al., 2010) to monitor the drift of instrumental bias and the external (spot-to-spot) reproducibility. External reproducibility, which represents the uncertainty of individual analyses of unknowns (Kita et al., 2009), was typically ~0.4, ~0.3, and ~0.4‰ (2SD) for $\delta^{17}O$, $\delta^{18}O$, and $\Delta^{17}O$, respectively. Olivine and pyroxene form solid solutions series that show systematic difference in instrumental biases in $\delta^{18}O$ (e.g., Tenner et al., 2013), which are calibrated using three olivine ($Fo_{100,\ 89,\ 60}$) and three low-Ca pyroxenes ($En_{97,\ 85,\ 70}$) and one diopside ($En_{50}Wo_{50}$) standard (Kita et al., 2010; Nakashima et al., 2013) that cover the range of chemical compositions observed in olivine and pyroxene in Kaba chondrules.

2.3. Selection of chondrules and positions of SIMS analysis

To minimize the sampling bias that is potentially introduced by preferential selection of chondrules by e.g., shape, texture, or degree of alteration, every chondrule larger or equal ~750 μm in diameter (or longest direction) was selected from a single polished thin section of Kaba (USNM 1052-1) for oxygen isotope analysis based on the evaluation of high-resolution BSE and SE images of the entire thin section. Due to scarcity of type II chondrules in Kaba, one small

(~150 µm) chondrule comprising FeO-rich olivine was included for SIMS analysis as well as one smaller chondrule (~600 µm) comprising FeO-rich pyroxene. All selected chondrules are labeled (K1 to K26) in the BSE mosaic image of the Kaba USNM 1052-1 thin section shown in Appendix EA1. At this point, exploratory SEM-EDS measurements were carried out to examine chemical zoning of minerals and to identify opaque phases. Per chondrule, at least 8 locations that are larger than 15 µm and free of cracks and inclusions were selected for SIMS analyses, preferably 4 for olivine and 4 for pyroxene, to be able to evaluate the isotopic homogeneity of individual chondrules. High-Ca pyroxene or plagioclase in the mesostasis of chondrules were not analyzed for oxygen three-isotopes, because they are usually smaller than 15 µm. The chemical compositions of minerals at each position were determined by EPMA and utilized later for instrumental bias correction of SIMS analyses. Finally, after SIMS analysis, each individual SIMS pit was imaged by SEM (see Appendix EA2) to evaluate whether cracks or inclusions were hit and whether the desired position was accurately sampled by the ion beam. Individual SIMS analyses were rejected from results if the primary beam overlapped two different mineral grains or an elevated OH signal in combination with visible cracks or cavities within pits indicate a compromised analysis.

2.4. Data reduction for host $\Delta^{17}O$ values of individual chondrules

In order to estimate representative oxygen isotope ratios of the last chondrule melt, Ushikubo et al. (2012) and Tenner et al. (2013) established a data reduction scheme to calculate the host $\Delta^{17}O$ value of a single chondrule as the mean value of multiple olivine and pyroxene analyses that are within a critical value from the mean. The same data reduction scheme was applied for chondrules in Kaba by using 0.6‰ ($\Delta^{17}O$) as the critical value, which is the mean 3SD of the bracketing San Carlos olivine standard during the 2 SIMS sessions. In a first step, the mean $\Delta^{17}O$ value from multiple analyses of an individual chondrule was calculated. If all data are within ±0.6‰ from the mean, this mean $\Delta^{17}O$ value is considered to represents that of the host chondrule. The host $\Delta^{17}O$ value should be determined by at least 2 data points. In a second step, for chondrules that contain data exceeding ±0.6‰ from the mean, a subset of data is selected, which preferably includes all pyroxene analyses and a new mean is calculated, only including this new subset. Subsequently, the subset is tested again for the variability criterion. The excluded olivine analyses, deviating more than 0.6‰ from the mean, are potential relict grains that may not reflect $\Delta^{17}O$ values of the final chondrule melt.

The host $\delta^{17}O$ and $\delta^{18}O$ values are calculated with the same subset of analyses that were used for calculating the host $\Delta^{17}O$ values. Uncertainties (at 95% confidence level) reported for host $\delta^{17}O$ and $\delta^{18}O$ values comprise the propagation of three types of uncertainties related to the analysis of unknowns, the instrumental bias correction based on the bracket standard, and the ultimate uncertainty of SIMS oxygen isotope analyses: Uncertainties (unc.) are calculated as the sum of those three components that are (i) twice the standard error $\left(2\frac{SD}{\sqrt{n}}\right)$ of those analyses that constitute the mean, where SD is standard deviation of the unknown analyses or that of the standard bracket whichever larger, (ii) twice the standard error of the analyses of the corresponding San Carlos olivine bracket, and (iii) a fixed value to account for possible mass-dependent fractionation in mean isotope ratios because of sample geometry and topography, as well as the reproducibility of calibration standards (±0.3‰ for $\delta^{18}O$, ±0.15‰ for $\delta^{17}O$, Kita et al., 2009, 2010). Uncertainties of host $\Delta^{17}O$ values only consider components (i) and (ii).

3. RESULTS

3.1. Petrography of chondrules

In the Kaba thin section, 7 type IA (<10% modal abundance of low-Ca pyroxenes), 3 type IB (<10% olivine), 14 type IAB, 1 type IIA, and 1 type IIB were analyzed for oxygen isotope compositions. The two individual chondrules K8 and K9 are part of one compound object and discussed together as chondrule K8+9 (Fig. 1a). Petrographic descriptions of each chondrule analyzed in this study is presented in the Appendix EA3. Chondrule sizes range from 0.6 – 3mm (diameter or longest direction); the type IIA chondrule is considerably smaller (0.15mm). Throughout this paper no distinction is made between complete chondrules and chondrule fragments. General textures of most investigated chondrules are best described as porphyritic.

Some type IAB chondrules show a predominately concentric layering. In particular, concentric layering within individual chondrules is well developed in the compound chondrule K8+9 (Fig. 1a), as well as in chondrules K1 (Fig. 1b) and K20 (Appendix EA1 , Page 20). In these examples, inner portions of chondrules comprise olivine, mesostasis, and in the case of the individual chondrule K8 also abundant opaque phases. Inner portions are mantled by pyroxenes, often containing olivine inclusions, and are enclosed with fine-grained rims dominated by pyroxene and dispersed opaque phases. The texture and mineralogy of the irregular-shaped chondrule K12 (see Appendix EA1, Page 12) resembles those of these fine-grained rims. Textures of the type IAB chondrules K3 and K19 (see Appendix EA1) indicate a similar concentric layering but fine-grained rims are absent.

In general, olivine occurs in type I chondrules (i) as anhedral grains (e.g., K3, K5, K8+9) or, rarely, as euhedral phenocrysts (K1) and small euhedral crystals in mesostasis (K4), (ii) in the form of irregular-shaped olivine masses (e.g., K19; K22, Fig. 1c), and (iii) as small euhedral grains poikilically enclosed in low-Ca pyroxene (e.g., K1, K24; K11, Fig. 1d). In type IA chondrules, olivine grains can be coarse-grained and embedded in varying amounts of interstitial mesostasis (K7, K10; K16, Fig. 1e). Chondrule K6 (IA) comprises olivine that contains metal grains, typical for "dusty olivine" relicts. Except for its occurrence in fine-grained rims, low-Ca pyroxene is usually subhedral (or even euhedral) and often exhibits a poikilitic texture caused by small individual inclusions (e.g., K11, K15, K24) or clusters of olivine grains (K13). The type IIB chondrule K25 comprises subhedral pyroxene that exhibits thin (<20μm) overgrows of olivine (K25, Fig. 1f).

Chondrules contain varying amounts of opaque phases (e.g., high abundance: K11, K12, K14, K23; low: K3, K7, K16, K22) that are evenly distributed within chondrules (e.g., K11, K12) or localized at their margins (e.g., K8+9, Fig 1a; K16, Fig. 1e). In chondrule K8+9, larger blobs of opaque phases are abundant at the interface of chondrule interior and rim (Fig. 1a). As confirmed by SEM-EDS analyses, opaque phases are mainly magnetite, Fe-Ni sulfides, and, rarely, Fe-Ni alloys (only in K1). The mesostasis is altered in most of the chondrules and comprises abundant phyllosilicates that probably replaced glassy mesostasis and plagioclase (Fig. 1c). High-Ca pyroxene often forms euhedral overgrows on low-Ca pyroxenes (Fig. 1c), sometimes also worm-like intergrow textures with plagioclase (see Appendix EA1, Page 14).

3.2. Mineral chemistry of olivine, pyroxene, and mesostasis phases

Mg#'s of olivine in type I chondrules are restricted to a narrow range between 98.5 and 99.8 (99.3 ±0.58, 2SD) and zoning caused by thermal metamorphism is insignificant (complete set of EPMA analyses in Appendix EA4). Thin FeO-rich halos around opaques or small holes in olivine, once filled by opaque minerals, are evidence for small-scale diffusion and excluded from analyses. Some olivine in chondrule K1 shows higher than typical Cr_2O_3 (up to 0.69wt%) and MnO (up to 0.49wt%) values compared to the mean of all olivine analyses (Cr_2O_3: 0.36 ±0.27wt%; MnO: 0.18 ±0.25wt%; 2SD). Chondrules K3, K7, and K22 contain olivine grains that yield CaO contents slightly higher than 0.5wt% (up to 0.59wt%). Olivine in the type IIA chondrule (K26) is zoned in Fe content and yields Mg#'s of 66.2 and 57.7 in the center and close to margins, respectively. The thin olivine overgrowths on pyroxene in the type IIB chondrule (K25) possess Mg#'s of about 83.

Low-Ca pyroxene ($Wo_{<3}$) is Fe-poor (mean Mg# type I: 99.1 ±0.51, 2SD) and shows the characteristic twinning of clinoenstatite when observed under crossed polarizers. In addition to low-Ca pyroxene, some type I chondrules (K5, K6, K8+9, K10, K13, K16) contain "intermediate pyroxene" (IntPx) often associated with mesostasis and distinguished from low-Ca pyroxene by higher Wo contents ($Wo_{3\text{-}5}$); lamellar twins are often absent in intermediate pyroxene. The fine-grained rim enclosing chondrules K8 and K9 comprises low-Ca and intermediate pyroxene. In chondrule K10, intermediate and high-Ca pyroxenes in the mesostasis are the only pyroxenes; in chondrule K16, low-Ca pyroxene is only present in insignificant amounts at chondrule margins whereas intermediate pyroxene fills interstitials of coarse olivine grains (Fig. 1e). Pyroxene in the type IIB chondrule (K25, Fig. 1f) is $En_{85}Fs_{14}Wo_1$ (Mg#: 85.7). In general, high-Ca pyroxenes ($En_{55\text{-}65}Fs_{<2}Wo_{34\text{-}44}$) that coexist with plagioclase ($An_{91\text{-}98}$) in the mesostasis of several chondrules can be considered as aluminian augites (Al > 0.1 apfu, atoms per formula unit). In these aluminian augites, the $Ca(R^{3+})AlSiO_6$ component, where R^{3+} is predominately Al, can exceed 15 mol% in a few cases. Ti contents of high-Ca pyroxenes are low (<0.05 apfu).

3.3. Oxygen three-isotope ratios

A total of 235 SIMS oxygen isotope analyses of olivine (133) and pyroxene (102) were performed. Thereof 16 had to be rejected from final results, mostly because (i) the spot area covered two different phases (e.g., K1: 98.Ol, 104.Lpx; see Appendix EA2, Page 1), (ii) abundant cracks (e.g., K4: 234.Lpx), (iii) the beam hit cavities in grains (e.g., K23: 309.Ol) or (iv) due to other surface imperfections. SIMS analyses are referred to in this paper by citing the chondrule identifier, followed by the analysis number and an abbreviation of the mineral analyzed. The complete oxygen three-isotope dataset of this study, including rejected analyses, is provided in Appendix EA5. Individual oxygen three-isotope diagrams of all analyzed chondrules are given in Appendix EA6.

Most oxygen isotope ratios of olivine and pyroxene plot either on the PCM or in between the PCM and CCAM lines (Fig. 2). The $\delta^{18}O$ and $\delta^{17}O$ values of all individual analyses range from ≈ –36‰ to +4‰ and –38‰ to +2‰, respectively ($\Delta^{17}O$ ≈ –19‰ - 0‰). Some of the most ^{16}O-rich analyses (e.g., $\Delta^{17}O$ ≈ –15‰, K4: 235.Ol, 236.Ol) show internal errors (derived from cycle-by-cycle variations within a single spot analysis) that are larger than typical (< 0.5‰), indicating heterogeneous oxygen three isotope ratios within an analyzed volume. Typical olivine and pyroxene in type I chondrules yield $\delta^{18}O$ and $\delta^{17}O$ values in between –12‰ and –1‰ and from –15‰ to –5‰, respectively ($\Delta^{17}O$ ≈ –8‰ - –3‰.). Pyroxene in the type IIB ($\delta^{18}O$: +3.7‰ - +4.0‰, $\delta^{17}O$: +2.0‰ - +2.1‰, $\Delta^{17}O$: 0.0‰ - +0.2‰) and olivine in the FeO-rich type IIA chondrule ($\delta^{18}O$: +2.6‰ - +2.9‰, $\delta^{17}O$: –1.1 - –0.4‰, $\Delta^{17}O$: –2.5‰ - –1.9‰) are ^{16}O-poor compared to those in type I chondrules. Analyses of olivine overgrowths on pyroxene of the type IIB chondrule (K25: 327.Ol, 328.Ol) have been rejected because of irregular SIMS pits, yet their

$\Delta^{17}O$ values ($\Delta^{17}O$: 0.09 ±0.01‰, n=2, 2SD) are indistinguishable within analytical uncertainty from those of the pyroxene (0.06 ±0.19‰, n=3, 2SD) in the same chondrule.

3.4. The presence of isotopic relict grains and host chondrule $\Delta^{17}O$ values

Figure 3 provides oxygen three-isotope diagrams for selected chondrules and Fig. 4 shows $\Delta^{17}O$ values of olivine and pyroxene as well as mean chondrule $\Delta^{17}O$ values. For all chondrules examined, at least 3, but usually more than 7 analyses are indistinguishable within analytical uncertainties (Fig 3a-g). 11 out of 25 chondrules comprise olivine analyses that are variable in $\Delta^{17}O$ values beyond the threshold, and some of them are considered to represent analyses of relict grains. Most relict olivine grains are ^{16}O-rich relative to their host, but in some chondrules (see Fig. 4; K18, K16) relict olivine grains are ^{16}O-poor relative to the corresponding host. Olivine analyses in chondrules K5, K13, and K16 form clusters with mean $\Delta^{17}O$ values that are distinguishable from those of the corresponding pyroxene clusters. Therefore, in these cases, the host $\Delta^{17}O$ values are determined by using only pyroxene analyses although a part of the olivine analyses in chondrules K5 and K13 are within the variability threshold. In chondrules K6, K8+9, and K24, the internal variability of $\Delta^{17}O$ is marginal compared to the threshold of 0.6‰.

Most chondrules in the Kaba 1052-1 thin section (21 out of 25) yield almost continuous host $\Delta^{17}O$ values in between –6.1 and –3.9‰ ($\delta^{18}O$: –6.9 - –2.1‰, $\delta^{17}O$: –9.7 - –5.0‰, see Fig. 4 and Table 1). Chondrules K18 (IA) and K23 (IAB) possess the lowest host $\Delta^{17}O$ values of –8.3‰ ($\delta^{18}O$: –12.0‰, $\delta^{17}O$: –14.5‰) and –7.8‰ ($\delta^{18}O$: –7.0‰, $\delta^{17}O$: –11.4‰), respectively. The type IIB chondrule (K25) and the type IIA chondrule (K26) show the most ^{16}O-poor compositions with host $\Delta^{17}O$ values of 0.1‰ ($\delta^{18}O$: 3.8‰, $\delta^{17}O$: 2.0‰) and –2.2‰ ($\delta^{18}O$: 2.7‰, $\delta^{17}O$: –0.8‰), respectively.

4. DISCUSSION

4.1. Evaluation of host chondrule oxygen isotope ratios

The primary aim of this SIMS oxygen isotope study of olivine and low-Ca pyroxene phenocrysts is to determine the oxygen isotope ratios of the last chondrule-forming melt that would record the average oxygen isotope ratios of the local dust-enriched disk. For clarity, the term “last chondrule-forming melt” is used here to refer to the product of the last major melting event that is recorded in most chondrules of one chondrite. These melts interacted with the ambient gas before or during crystallization of chondrule minerals (e.g., Tissandier et al., 2002; Hewins and Zanda, 2012; Nagahara and Ozawa, 2012; Di Rocco and Pack, 2015; Marrocchi and Chaussidon, 2015) and there is evidence that chondrule phenocrysts and evolved melts were not in chemical equilibrium (e.g., Libourel et al., 2006). This disequilibrium, in turn, raises some doubts whether $\Delta^{17}O$ values of olivine and low-Ca are actual representative for those of the last chondrule-forming melt. However, Ushikubo et al. (2011) showed for Acfer 094 (ungr. CC), the most pristine carbonaceous chondrite known to date, that chondrule phenocrysts (excluding relicts) and mesostasis phases such as high-Ca pyroxenes, plagioclase, and glass are indistinguishable in respect to $\Delta^{17}O$ values. Also, high-Ca pyroxenes, plagioclase, and olivine show indistinguishable $\Delta^{17}O$ values in chondrules from two CR chondrites (Tenner et al., 2015) and Yamato-82094 (ungr. CC, Tenner et al., 2017). Moreover, it is likely that systematically higher $\Delta^{17}O$ values of chondrule glass in Semarkona (LL, Kita et al., 2010) or plagioclase in Kaba (CV, Krot and Nagashima, 2016) are due to parent body processes and not caused by gas-melt exchange during plagioclase crystallization or glass formation.

Porphyritic chondrules can contain mineral grains that didn’t completely melt during the chondrule-forming event and are identified as relict grains either by chemical compositions and/or isotope ratios (e.g., Jones et al., 2004; Kunihiro et al., 2004; Krot et al., 2006; Berlin et al., 2011; Rudraswami et al., 2011; Ushikubo et al., 2012; Schrader et al., 2013; Tenner et al., 2013). Relict olivine grains predate “host” minerals that crystallized from the final chondrule melt (Nagahara, 1981; Jones, 1996; Wasson and Rubin, 2003). Classical examples of those relict olivine are ^{16}O-rich forsteritic cores in type II chondrules of carbonaceous chondrites (e.g., Yurimoto and Wasson, 2002; Kunihiro et al., 2004, 2005; Rudraswami et al., 2011; Ushikubo et al., 2012; Schrader et al., 2013; Tenner et al., 2013). However, in most of the cases, isotopically distinct olivine relict grains are chemically and petrographically indistinguishable from other olivine of the same chondrule and only identified by SIMS analyses at sub-‰ precisions (e.g., Rudraswami et al., 2011; Ushikubo et al., 2012; Tenner et al., 2013, 2015, 2017). In order to deduce representative oxygen isotope ratios of the chondrule-forming environment, it has proven useful to define mean “host” oxygen isotope ratios. These host values have analyses of those isotopic relict grains excluded from chondrule means (e.g., Kunihiro et al., 2004; Ushikubo et al., 2012; Tenner et al., 2017).

In 11 of 22 chondrules, analyzed olivine grains are indistinguishable from pyroxene in the same chondrule, i.e., chondrules are relict grain-free and contain both minerals. The total number of chondrules cited here excludes chondrules K23 and K25 where no valid olivine or pyroxene analyses, respectively, are available as well as K26 that doesn't contain pyroxene. Moreover, 19 out of 22 chondrules, shown in Fig. 5a, are either relict grain-free or contain at least one olivine with Δ^{17}O values indistinguishable from pyroxene of the same chondrule; the remainder comprises three chondrules, K5, K13, and K16, where all olivine are considered to represent relict grains. Since olivine is the liquidus phase succeeded by low-Ca pyroxene during crystallization of type I chondrule melts, there is a possibility that a changing melt Δ^{17}O value during crystallization would be reflected in differing $\Delta^{17}O$ values of both minerals, e.g., higher $\Delta^{17}O$ values of pyroxenes relative to those of olivine (e.g., Chaussidon et al., 2008); such systematic relationship was clearly not observed in this study. It is therefore suggested that olivine and pyroxene crystallized from a homogenized melt in respect to $\Delta^{17}O$ and that the mean chondrule $\Delta^{17}O$ values of chondrule olivine and pyroxene can be used as a proxy for those of the last chondrule-forming melt.

There could be, however, a tendency of olivine to show slightly higher $\delta^{18}O$ values than pyroxene of the same chondrule, but caution is advised because variations are within analytical uncertainties (see Fig. 5b). Similar observations were made earlier for different chondrites (Tenner et al., 2013, 2015) and attributed to evaporative loss of light isotopes before olivine crystallization followed by re-condensation of light isotopes before or during pyroxene crystallization (Tenner et al, 2015). Since such processes result only in mass-dependent fractionation, chondrule $\Delta^{17}O$ values and conclusions based thereof are not affected by this type of gas-melt interaction.

Mean chondrule $\Delta^{17}O$ values determined for Kaba are independent of the modal abundance of olivine and pyroxene as shown in Fig. 6 which is in line with previous SIMS oxygen isotope studies on unequilibrated carbonaceous chondrites (Rudraswami et al., 2011; Ushikubo et al., 2012; Tenner et al., 2013, 2015). Apart from the Mg#'s, this study found no connection between oxygen isotope ratios and chemical compositions of olivine or pyroxene. For example, there exists no systematic difference of pyroxene $\delta^{17}O$, $\delta^{18}O$, or $\Delta^{17}O$ depending on the Wo content (i.e., low-Ca pyroxene vs. Intermediate pyroxene). In agreement with previous SIMS oxygen isotope studies on chondrule in carbonaceous chondrites (e.g., Rudraswami et al., 2011; Ushikubo et al., 2012; Tenner et al., 2015), most host chondrule $\Delta^{17}O$ values plot on the PCM line or between the PCM and CCAM lines (see Fig. 6); notable exceptions are chondrules K25 (type IIB) and K23 (IAB). In the latter case (K23), isotopic compositions of olivine are potentially fractionated.

4.2. Consistent Mg#'s of chondrule olivine and pyroxene

Pristine oxygen isotope ratios and Mg#'s are a precondition for reliable conclusions about the chondrule-forming environment and consistent Mg#'s of olivine and pyroxenes are an important indicator whether thermal metamorphism could have disturbed primary values. According to the equilibrium condensation model of Ebel and Grossmann (2000), olivine and orthopyroxene initially show similar Mg#'s of about 98 at the time the last melt disappears (Ebel and Grossmann, 2000, therein Fig. 8, dust enrichment factor: 100). Due to diffusive exchange with Fe-rich minerals, olivine and pyroxene could become more FeO-rich during parent body metamorphism. Importantly, the interdiffusion coefficient of Fe and Mg in olivine is about 2 log units larger than in orthopyroxene (e.g., Dohmen and Chakraborty, 2007; Dohmen et al., 2016, and references therein), i.e., diffusion rates are higher in olivine than in orthopyroxene. Therefore, low degrees of thermal metamorphism manifests itself first in elevated olivine Mg#'s whereas pyroxene Mg#'s remain unchanged. Further, because diffusion of Fe and Mg is fast relative to that of oxygen (Dohmen and Chakraborty, 2007), matching Mg# indicate that both minerals probably record primary oxygen isotope ratios. However, it should be noted that fluids could have enhanced oxygen diffusion in those silicates (Farver, 2010, and references therein). In this study we found consistent Mg#'s of most olivine pyroxenes within individual chondrules from Kaba, providing evidence for unaltered Mg-Fe ratios and $\Delta^{17}O$ values. Those values can now be used to infer possible dust enrichment and ice enhancement factors of the CV chondrule-forming region.

4.3. Relating oxygen isotope compositions of chondrules to levels of dust enrichment in the chondrule forming region

Tenner et al. (2015) proposed a simple yet powerful model to relate the $\Delta^{17}O$ values and Mg#'s of host chondrules to the extent of dust enrichment and the contribution of distinct precursor oxygen reservoirs. The oxygen isotope characteristics of host chondrules are described by an oxygen isotope mass balance that involves Solar gas ($\Delta^{17}O$ = –28.4 ‰), anhydrous silicate dust (–5.9‰) as well as organics (+11.8‰) and H_2O ice (+5.1‰) in the dust as precursor oxygen reservoirs. At a given amount of water ice, chondrule $\Delta^{17}O$ values strongly increase with rising dust enrichment but continue to increase only marginally at dust enrichment factors higher than 100 because at these conditions, mass balance is dominated by nearly constant amounts of oxygen from the anhydrous silicate precursor dust and the water ice.

For instance, if a chondrule formed in a region with 100 times (CI) dust enrichment (H/O ~37) relative to Solar nebula values, 43% and 53% of the oxygen in the chondrule would come from precursor anhydrous silicates and water ice in the dust, respectively; only a minor fraction of 4% would be inherited from the Solar gas and organics in the dust (Tenner et al., 2015, see their Table 3). Hence, when applying the model originally calibrated for CR chondrules to chondrules in CV chondrites, new $\Delta^{17}O$ values for the precursor silicates and water ice need to be defined whereas a difference in $\Delta^{17}O$ values for the organics in both regions can be ignored. Following Tenner et al. 2015, oxygen isotope ratios for both reservoirs are defined based on the assumption that the lowest measured chondrule $\Delta^{17}O$ values (mean of K18 and K23: –8.0‰) are representative for the effective $\Delta^{17}O$ value of the anhydrous precursor silicates and that chondrules with higher $\Delta^{17}O$ values are formed by addition of ^{16}O-poor water ice. Since type II chondrules likely formed at highly dust-enriched conditions, the $\Delta^{17}O$ value of the water ice is calculated using the measured $\Delta^{17}O$ value of chondrule K26 (–2.2‰, type II) in the following way: at a dust enrichment factor of 1000, the mass balance involves oxygen from the sources water ice, anhydrous silicate dust, and organics in the following proportions 54:44:2 (Tenner et al., 2015); solving the mass balance for the $\Delta^{17}O$ value of water ice, results in a value of +2‰.

Host chondrule $\Delta^{17}O$ and Mg#'s from Kaba are shown in Fig. 7 in combination with modeled dust and ice enrichment factors. Error bars for Mg#'s denote maximum-minimum ranges including olivine and pyroxene analyses in individual chondrules of Kaba. Data suggests that higher chondrule Mg#'s correlate with lower $\Delta^{17}O$ values which is in line with results for chondrules from CR chondrites (Schrader et al., 2013, 2014, 2017; Tenner et al., 2015). According to the model of Tenner et al. (2015), values of type I host chondrules in Kaba correspond to low dust enrichment factors between 50× and 100× and low amounts of water ice (anhydrous CI dust to 0.6× the nominal amount of ice in dust of CI composition) in the dust. The type IIB chondrule could have formed at 300× dust enrichment and ~3× water ice. However, formation of this chondrule might be unrelated to that of other chondrules because $\delta^{18}O$ values are fractionated in such a way that analyses plot off the PCM and on the TF line. This distinguishes them from analyses of all other chondrules and suggests that at least one different precursor reservoir contributed to their formation (e.g., Clayton et al., 1983; Tenner et al., 2015). The type II chondrule K26 possibly formed at dust enrichments of 2000×. Results from this study support the idea that Mg#'s and $\Delta^{17}O$ values may be correlated even for very Mg-rich chondrules with Mg#'s above 99. For these reducing conditions ($\log_{fO2}$: IW – 3.5), increasing $\Delta^{17}O$ values in combination with decreasing Mg#'s may be due to a small increase in the dust enrichment factor or water ice contents or a combination of both parameters (see Fig. 7), as noted by, e.g., Tenner et al. (2015).

Ice enhancement and, to a lower degree, dust enrichment factors inferred from chondrule $\Delta^{17}O$ values vary with the assumed isotope ratios of the contributing reservoirs. For example, overestimating the $\Delta^{17}O$ value of anhydrous silicate dust in the precursor by 5‰ ($\Delta^{17}O$ = –12‰ instead of –8‰) has only a limited effect on inferred maximum dust enrichments (slight decrease) but increases the maximum estimated ice enhancement factor to 1× the nominal amount of ice in CI dust (type I chondrules), when keeping other parameters constant. As discussed by Tenner et al. (2015), alternative $\Delta^{17}O$ values of water ice (e.g., +80‰) can significantly decrease the inferred ice enhancement factor while only moderately affecting dust enrichment factors, e.g., shifting maximum enrichment factors obtained for Kaba type I chondrules from 100× to 200× CI dust relative to Solar abundance. In conclusions, dust enrichment factors inferred from chondrules in Kaba are likely reasonable estimates for the chondrule forming environment, while ice enhancement factors are less accurately known and sensitive to the applied $\Delta^{17}O$ values of reservoirs.

In the scope of the model by Marrocchi and Chaussidon (2015), relict olivine grains represent the direct silicate precursor material for the individual chondrule they are included in. Differences between isotope ratios of individual chondrules are, consequently, due to isotopically distinct precursor olivine rather than due to influence of ^{16}O-poor water ice. Further, Marrocchi and Chaussidon (2015) suggest that, if present, isotopic disequilibrium between chondrule olivine and pyroxene ($\Delta^{18}O_{px-ol}$) represents a possible proxy for dust enrichment in the chondrule-forming region. Accordingly, isotopically homogeneous chondrules would indicate high (>100 times) dust enrichments. A $\Delta^{18}O_{px-ol}$ of approximately +1.5 like observed in chondrules K5 and K13 would amount to dust enrichments smaller than 5×, considering precursor olivine of –5‰ (Marrocchi and Chaussidon, 2015, see their Table S1). Within the framework of that model, ^{16}O-poor relict olivine as a source for ^{16}O-rich pyroxene as found in chondrule K16 is only conceivable with ^{16}O-rich gas and extremely low dust enrichment factors (< 0.001). The model predictions such as the low dust enrichment factors for the three chondrules are based on the explicit assumption that most olivine are relict grains. Although it can't be ruled out that some olivine grains with $\Delta^{17}O$ values similar to pyroxenes are actually relict grains, there is recent chemical and isotopic evidence from chondrules in CR chondrites (Schrader et al., 2014) that argue against such a scenario where most olivine in type I chondrules are relict (e.g., Libourel and Krot, 2007; Libourel and Chaussidon, 2011).

4.4. Comparison to data from the Allende CV3 and other carbonaceous chondrites

It can be seen from the previous discussion that host chondrule $\Delta^{17}O$ values in combination with mean Mg#'s provide important information about the contribution of different oxygen reservoirs to chondrule formation. With histograms presented in Fig. 8, host chondrule $\Delta^{17}O$ values of Kaba are compared to those of various groups of carbonaceous chondrites in order to identify common chondrule populations. Literature data in Fig. 8 are selected based on the following criterions: (1) The precision of individual chondrule means are small compared to bin size (<0.5‰), (2) the chondrule means were obtained from multiple analyses (n>4) of single chondrule at sub‰ precision in order to exclude obvious relict olivine analysis, and (3) the total number of chondrules in the dataset are statistically meaningful (n≥20) and generally cover a representative set of chondrule types. It is important to note that frequencies of host $\Delta^{17}O$ values can be prone to misinterpretations because available chondrule data may not be completely representative for the meteorite. In many studies, chondrules are primarily selected based on the size of mineral grains due to spatial resolution of the SIMS method. For example, grain size limitations might have biased Allende data towards type IA chondrules (Rudraswami et al., 2011). Also, minor chondrule types, such as type II chondrules in carbonaceous chondrites and Al-rich chondrules are often over-selected compared to their actual representative abundances (e.g., Connolly and Huss, 2010; Ushikubo et al., 2012; Schrader et al., 2013; Tenner et al., 2017).

Histograms of host chondrule $\Delta^{17}O$ values of Kaba, Allende, Yamato 81020, two CRs, Yamato 82094, and Acfer 094 (for references see Fig. 8) show at least one common mode of $\Delta^{17}O$ values in between –6‰ and –4‰. Yamato 81020, the CR chondrites, and Acfer 094 also contain a significant fraction of chondrules with $\Delta^{17}O$ values of ~ –2‰, which are observed in Kaba, Allende, and Yamato 82094 as minor components. Except for Yamato 81020, all carbonaceous chondrites mentioned in Fig. 8 contain chondrules with $\Delta^{17}O$ values of about 0‰. Only the Kaba, Acfer 094, and Yamato 82094 chondrites contain chondrules with $\Delta^{17}O$ values lower than –7‰. In general, type I chondrules are ^{16}O-rich in comparison to type II chondrules and show a negative correlation between chondrule Mg# and $\Delta^{17}O$ values, as indicated by different grey tones in Fig. 8. More precisely, excluding the two CR chondrites, most type I chondrules possess host $\Delta^{17}O$ values in the range between –6‰ and –4‰ with a minor mode at about –2‰ that mainly comprises chondrules with Mg#'s below 98. In contrast to the strong bimodal host $\Delta^{17}O$ values from the Acfer 094 and Yamato 81020 chondrites, data on type I chondrules from the CR chondrites suggest a continuum of $\Delta^{17}O$ values ranging from –6 to –1‰. At large, it appears that type II chondrules only possess $\Delta^{17}O$ values higher than –4‰ whereas type I chondrules can show host $\Delta^{17}O$ values from –10‰ up to 0‰.

Analyzed chondrules from the Kaba CV3 chondrite differ from those in the aforementioned chondrites, especially Allende, in two major aspects: First, host chondrule Mg#'s are consistently above 98 and, second, there exist no type I chondrules in Kaba that show $\Delta^{17}O$ values higher than ~ –3‰. In Allende chondrules, the difference in Mg#'s is due to secondary processes, so that high Mg#'s among many Kaba chondrules represent the primary characters of chondrules in CV. However, the lack of type I chondrules with $\Delta^{17}O > -3‰$ among chondrules in Kaba studied here could be due to sampling bias because only chondrules from a single thin section of Kaba were analyzed. Precursors of type I chondrules with ^{16}O-poor signature ($\Delta^{17}O > -3‰$) are indicated from the analysis of chondrule K16 (IA, Fig. 1e), in which relatively ^{16}O-rich pyroxene analyses define the host value ($\Delta^{17}O = -5.03 \pm 0.27‰$, unc.) by excluding ^{16}O-poor ($\Delta^{17}O = -1.57 \pm 0.22‰$, unc.) relict olivine analysis. Such ^{16}O-poor relict olivine was also found in Allende chondrules (Rudraswami et al., 2011).

5. CONCLUSIONS

Olivine and pyroxene in chondrules from the Kaba USNM 1052-1 thin section were analyzed for oxygen three-isotopes (SIMS) and mineral chemistry (EPMA) in order to evaluate the degree of isotopic homogeneity in chondrules and the relationship of chondrule $\Delta^{17}O$ values and Mg#'s. More than one third of the analyzed chondrules in the Kaba CV3 contain isotopic olivine relict grains that are generally ^{16}O-rich relative to chondrule means; however, three chondrule also comprise ^{16}O-poor relict grains. Excluding those isotopic relicts, mean chondrule $\Delta^{17}O$ values were calculated and it was demonstrated for most of the chondrules that olivine and pyroxene are isotopically indistinguishable and, consequently, that both minerals likely crystallized from the last chondrule-forming melt.

Except for two type II chondrules, the analyzed thin section only contains Mg-rich chondrules with high and uniform Mg#'s (host: 99.6 – 98.8). Consistent Mg#'s of olivine and pyroxene in individual chondrules support the interpretation that Kaba was only marginally affected by thermal metamorphism. The majority of type I chondrules possesses host $\Delta^{17}O$ values in the range between $-6‰$ and $-4‰$ and only two type I chondrules show more ^{16}O-rich compositions (~ –8‰). The type IIB and IIA chondrules are relatively ^{16}O-poor and yield $\Delta^{17}O$ values of 0‰ and –2‰, respectively. The $\Delta^{17}O$ values of type I chondrules in Kaba tend to increase continuously with decreasing Mg#'s.

In conclusion, type I chondrules in the Kaba CV3 chondrite are witnesses of an oxygen reservoir with an effective $\Delta^{17}O$ value of approximately –5‰ which is also commonly found in other groups of carbonaceous chondrites (e.g., Jones et al., 2004; Krot et al., 2006; Libourel and Chaussidon, 2011; Rudraswami et al., 2011; Ushikubo et al., 2013; Tenner et al., 2013, 2015; Schrader et al., 2014). Interestingly, host $\Delta^{17}O$ values of type I chondrules in Kaba don't show a pronounced bimodal distribution as it is evident for other carbonaceous chondrites such as Acfer 094 and Yamato 81020. At this point it is not clear whether the predominance of $\Delta^{17}O$ values in between –6‰ and –4‰ is an exclusive property of the investigated thin section or representative for Kaba in general.

If the analyzed chondrules in Kaba are representative of CV chondrites, the correlation of $\Delta^{17}O$ and Mg#'s points to similar principals that governed formation of type I chondrules in CV and CR chondrites. This includes a possible involvement of water ice as an oxidizing ^{16}O-poor agent. Inferred dust enrichment factors for the local disk environment are only moderately high (50-100×) and dust was almost anhydrous (anhydrous to 0.6× the nominal ice in dust of CI composition), based on investigations of type I chondrules in the Kaba CV3.

ACKNOWLEDGEMENTS

We thank Glenn MacPherson (National Museum of Natural History, Smithsonian Institution) for the allocation of Kaba thin section for this study. We are grateful to John Fournelle for help with EPMA measurements, Jim Kern for SIMS support, and Nöel Chaumard for discussion. Reviews of Devin Schrader and two anonymous reviewers significantly improved the manuscript. This work is supported by NASA Cosmochemistry Program (NNX14AG29G). WiscSIMS is partly supported by NSF (EAR13-55590).

REFERENCES

Alexander C. M. O.'D. (2004) Chemical equilibrium and kinetic constraints for chondrule and CAI formation conditions. *Geochim. Cosmochim. Acta* **68**, 3943–3969.

Berlin J., Jones R. H. and Brearley A. J. (2011) Fe-Mn systematics of type IIA chondrules in unequilibrated CO, CR, and ordinary chondrites. *Meteorit. Planet. Sci.* **46**, 513–533.

Bonal L., Quirico E., Bourot-Denise M. and Montagnac G. (2006) Determination of the petrologic type of CV3 chondrites by Raman spectroscopy of included organic matter. *Geochim. Cosmochim. Acta* **70**, 1849–1863.

Busemann H., Alexander C. M. O.'D. and Nittler L. R. (2007) Characterization of insoluble organic matter in primitive meteorites by microRaman spectroscopy. *Meteorit. Planet. Sci.* **42**, 1387–1416.

Chaussidon M., Libourel G. and Krot A. N. (2008) Oxygen isotopic constraints on the origin of magnesian chondrules and on the gaseous reservoirs in the early Solar System. *Geochim. Cosmochim. Acta* **72**, 1924–1938.

Choi B.-G., Krot A. N. and Wasson J. T. (2000) Oxygen-isotopes in magnetite and fayalite in CV chondrites Kaba and Mokoia. *Meteorit. Planet. Sci.* **35**, 1239–1248.

Ciesla F. J. (2005) Chondrule-forming Processes – An Overview. In *Chondrites and the protoplanetary disk* (eds. A. N. Krot, E. R. D. Scott and B. Reipurth). Astronomical Society of the Pacific, San Francisco, CA. pp. 811–820.

Clayton R. N. (1993) Oxygen Isotopes in Meteorites. *Annu. Rev. Earth Planet. Sci.* **21**, 115–149.

Clayton R. N. and Mayeda T. K. (1999) Oxygen isotope studies of carbonaceous chondrites. *Geochim. Cosmochim. Acta* **63**, 2089–2104.

Clayton R. N., Grossman L. and Mayeda T. K. (1973) A Component of Primitive Nuclear Composition in Carbonaceous Meteorites. *Science* **182**, 485–488.

Clayton R. N., Onuma N., Grossman L. and Mayeda T. K. (1977) Distribution of the pre-Solar component in Allende and other carbonaceous chondrites. *Earth Planet. Sc. Lett.* **34**, 209–224.

Clayton R. N., Onuma N., Ikeda Y., Mayeda T. K., Hutcheon I. D., Olsen E. J. and Molini-Velsko C. (1983) Oxygen isotopic compositions of chondrules in Allende and ordinary chondrites. In *Chondrules and their origins* (ed. E. A. King). Lunar and Planetary Institute, Huston, TX. pp. 37–43.

Connolly H. C., Jr. and Desch S. J. (2004) On the origin of the "kleine Kügelchen" called Chondrules. *Chem. Erde - Geochem.* **64**, 95–125.

Connolly H. C., Jr. and Huss G. R. (2010) Compositional evolution of the protoplanetary disk. *Geochim. Cosmochim. Acta* **74**, 2473–2483.

Di Rocco T. and Pack A. (2015) Triple oxygen isotope exchange between chondrule melt and water vapor. *Geochim. Cosmochim. Acta* **164**, 17–34.

Dohmen R. and Chakraborty S. (2007) Fe–Mg diffusion in olivine II. *Phys. Chem. Minerals* **34**, 409–430.

Dohmen R., Ter Heege J. H., Becker H.-W. and Chakraborty S. (2016) Fe-Mg interdiffusion in orthopyroxene. *Am. Mineral.* **101**, 2210–2221.

Donovan J. J. (2015) *Probe for EPMA v. 11.1.5.* Probe Software, Inc, Eugene, OR.

Ebel D. S. and Grossman L. (2000) Condensation in dust-enriched systems. *Geochim. Cosmochim. Acta* **64**, 339–366.

Farver J. R. (2010) Oxygen and Hydrogen Diffusion in Minerals. *Rev. Mineral. Geochem.* **72**, 447–507.

Fedkin A. V. and Grossman L. (2006) The Fayalite Content of Chondritic Olivine: Obstacle to Understanding the Condensation of Rocky Material. In *Meteorites and the Early Solar System II* (eds. D. S. Lauretta and H. McSween). University of Arizona Press, Tucson. pp. 279–294.

Fedkin A. V. and Grossman L. (2016) Effects of dust enrichment on oxygen fugacity of cosmic gases. *Meteorit. Planet. Sci.* **51**, 843–850.

Grossman J. N. and Brearley A. J. (2005) The onset of metamorphism in ordinary and carbonaceous chondrites. *Meteorit. Planet. Sci.* **40**, 87–122.

Hewins R. H. (1996) Chondrules and the protoplanetary disk: an overview. In *Chondrules and the protoplanetary disk* (eds. R. H. Hewins, R. H. Jones and E. R. D. Scott). Cambridge Univ. Press, Cambridge. pp. 3–9.

Hewins R. H. and Zanda B. (2012) Chondrules. *Meteorit. Planet. Sci.* **47**, 1120–1138.

Hua X., Huss G. R., Tachibana S. and Sharp T. G. (2005) Oxygen, silicon, and Mn-Cr isotopes of fayalite in the Kaba oxidized CV3 chondrite. *Geochim. Cosmochim. Acta* **69**, 1333–1348.

Jones R. H. (1996) FeO-rich, porphyritic pyroxene chondrules in unequilibrated ordinary chondrites. *Geochim. Cosmochim. Acta* **60**, 3115–3138.

Jones R. H., Leshin L. A., Guan Y., Sharp Z. D., Durakiewicz T. and Schilk A. J. (2004) Oxygen isotope heterogeneity in chondrules from the Mokoia CV3 carbonaceous chondrite. *Geochim. Cosmochim. Acta* **68**, 3423–3438.

Kimura M. and Ikeda Y. (1998) Hydrous and anhydrous alterations of chondrules in Kaba and Mokoia CV chondrites. *Meteorit. Planet. Sci.* **33**, 1139–1146.

Kita N. T., Ushikubo T., Fu B. and Valley J. W. (2009) High precision SIMS oxygen isotope analysis and the effect of sample topography. *Chem. Geol.* **264**, 43–57.

Kita N. T., Nagahara H., Tachibana S., Tomomura S., Spicuzza M. J., Fournelle J. H. and Valley J. W. (2010) High precision SIMS oxygen three isotope study of chondrules in LL3 chondrites. *Geochim. Cosmochim. Acta* **74**, 6610–6635.

Krot A. N. and Nagashima K. (2016) Evidence for Oxygen-Isotope Exchange in Chondrules and Refractory Inclusions During Fluid-Rock Interaction on the CV Chondrite Parent Body. *Meteorit. Planet. Sci. Suppl.* **51**, A249.

Krot A. N., Scott E. R. D. and Zolensky M. E. (1995) Mineralogical and chemical modification of components in CV3 chondrites. *Meteorit. Planet. Sci*. **30**, 748–775.

Krot A. N., Petaev M. I., Scott E. R. D., Choi B.-G., Zolensky M. E. and Keil K. (1998) Progressive alteration in CV3 chondrites. *Meteorit. Planet. Sci.* **33**, 1065–1085.

Krot A. N., Fegley B., Lodders K. and Palme H. (2000) Meteoritical and astrophysical constraints on the oxidation state of the Solar nebula. In *Protostars and Planets IV* (eds. V. Mannings, A. P. Boss and S. S. Russell). University of Arizona Press, Tucson. pp. 1019–1054.

Krot A. N., Yurimoto H., McKeegan K. D., Leshin L. A., Chaussidon M., Libourel G., Yoshitake M., Huss G. R., Guan Y. and Zanda B. (2006) Oxygen isotopic compositions of chondrules. *Chem. Erde - Geochem.* **66**, 249–276.

Krot A. N., Nagashima K., Ciesla F. J., Meyer B. S., Hutcheon I. D., Davis A. M., Huss G. R. and Scott E. R. D. (2010) Oxygen Isotopic Composition of the Sun and Mean Oxygen Isotopic Composition of the Protosolar Silicate Dust. *Astrophys. J.* **713**, 1159–1166.

Kunihiro T., Rubin A. E., McKeegan K. D. and Wasson J. T. (2004) Oxygen-isotopic compositions of relict and host grains in chondrules in the Yamato 81020 CO3.0 chondrite. *Geochim. Cosmochim. Acta* **68**, 3599–3606.

Kunihiro T., Rubin A. E. and Wasson J. T. (2005) Oxygen-isotopic compositions of low-FeO relicts in high-FeO host chondrules in Acfer 094, a type 3.0 carbonaceous chondrite closely related to CM. *Geochim. Cosmochim. Acta* **69**, 3831–3840.

Libourel G. and Krot A. N. (2007) Evidence for the presence of planetesimal material among the precursors of magnesian chondrules of nebular origin. *Earth Planet. Sc. Lett.* **254**, 1–8.

Libourel G. and Chaussidon M. (2011) Oxygen isotopic constraints on the origin of Mg-rich olivines from chondritic meteorites. *Earth Planet. Sc. Lett.* **301**, 9–21.

Libourel G., Krot A. N. and Tissandier L. (2006) Role of gas-melt interaction during chondrule formation. *Earth Planet. Sc. Lett.* **251**, 232–240.

Marrocchi Y. and Chaussidon M. (2015) A systematic for oxygen isotopic variation in meteoritic chondrules. *Earth Planet. Sc. Lett.* **430**, 308–315.

Morris M. A., Boley A. C., Desch S. J. and Athanassiadou T. (2012) Chondrule formation in bow shocks around eccentric planetary embryos. *Astrophys. J.* **752**, 27.

Nagahara H. (1981) Evidence for secondary origin of chondrules. *Nature* **292**, 135–136.

Nagahara H. and Ozawa K. (2012) The role of exchange reactions in oxygen isotope fractionation during CAI and chondrule formation. *Meteorit. Planet. Sci.* **47**, 1209–1228.

Nagahara H., Kita N. T., Ozawa K. and Morishita Y. (2008) Condensation of major elements during chondrule formation and its implication to the origin of chondrules. *Geochim. Cosmochim. Acta* **72**, 1442–1465.

Nagashima K., Krot A. N. and Huss G. R. (2015) Oxygen-isotope compositions of chondrule phenocrysts and matrix grains in Kakangari K-grouplet chondrite. *Geochim. Cosmochim. Acta* **151**, 49–67.

Nakashima D., Kimura M., Yamada K., Noguchi T., Ushikubo T. and Kita N. T. (2010) Study of chondrules in CH chondrites - I: oxygen isotope ratios of chondrules. *Meteorit. Planet. Sci. Suppl.* **45**, A148.

Nakashima D., Kita N. T., Ushikubo T., Noguchi T., Nakamura T. and Valley J. W. (2013) Oxygen three-isotope ratios of silicate particles returned from asteroid Itokawa by the Hayabusa spacecraft. *Earth Planet. Sc. Lett.* **379**, 127–136.

Rubin A. E. (2000) Petrologic, geochemical and experimental constraints on models of chondrule formation. *Earth Sci. Rev.* **50**, 3–27.

Rudraswami N. G., Ushikubo T., Nakashima D. and Kita N. T. (2011) Oxygen isotope systematics of chondrules in the Allende CV3 chondrite. *Geochim. Cosmochim. Acta* **75**, 7596–7611.

Schrader D. L., Connolly H. C., Jr., Lauretta D. S., Nagashima K., Huss G. R., Davidson J. and Domanik K. J. (2013) The formation and alteration of the Renazzo-like carbonaceous chondrites II. *Geochim. Cosmochim. Acta* **101**, 302–327.

Schrader D. L., Nagashima K., Krot A. N., Ogliore R. C. and Hellebrand E. (2014) Variations in the O-isotope composition of gas during the formation of chondrules from the CR chondrites. *Geochim. Cosmochim. Acta* **132**, 50–74.

Schrader D. L., Nagashima K., Krot A. N., Ogliore R. C., Yin Q.-Z., Amelin Y., Stirling C. H. and Kaltenbach A. (2017) Distribution of ^{26}Al in the CR chondrite chondrule-forming region of the protoplanetary disk. *Geochim. Cosmochim. Acta* **201**, 275–302.

Tenner T. J., Ushikubo T., Kurahashi E., Kita N. T. and Nagahara H. (2013) Oxygen isotope systematics of chondrule phenocrysts from the CO3.0 chondrite Yamato 81020. *Geochim. Cosmochim. Acta* **102**, 226–245.

Tenner T. J., Nakashima D., Ushikubo T., Kita N. T. and Weisberg M. K. (2015) Oxygen isotope ratios of FeO-poor chondrules in CR3 chondrites. *Geochim. Cosmochim. Acta* **148**, 228–250.

Tenner T. J., Kimura M. and Kita N. T. (2017) Oxygen isotope characteristics of chondrules from the Yamato-82094 ungrouped carbonaceous chondrite: Further evidence for common O-isotope environments sampled among carbonaceous chondrites. *Meteorit. Planet. Sci.* **52**, 268-294.

Tissandier L., Libourel G. and Robert F. (2002) Gas-melt interactions and their bearing on chondrule formation. *Meteorit. Planet. Sci.* **37**, 1377–1389.

Ushikubo T., Nakashima D., Kimura M., Tenner T. J. and Kita N. T. (2013) Contemporaneous formation of chondrules in distinct oxygen isotope reservoirs. *Geochim. Cosmochim. Acta* **109**, 280–295.

Wasson J. T. and Rubin A. E. (2003) Ubiquitous low-FeO relict grains in type II chondrules and limited overgrowths on phenocrysts following the final melting event. *Geochim. Cosmochim. Acta* **67**, 2239–2250.

Young E. D. and Russell S. S. (1998) Oxygen Reservoirs in the Early Solar Nebula Inferred from an Allende CAI. *Science* **282**, 452–455.

Yurimoto H. and Wasson J. T. (2002) Extremely rapid cooling of a carbonaceous-chondrite chondrule containing very ^{16}O-rich olivine and a ^{26}Mg-excess. *Geochim. Cosmochim. Acta* **66**, 4355–4363.

Yurimoto H., Krot A. N., Choi B.-G., Aleon J., Kunihiro T. and Brearley A. J. (2008) Oxygen Isotopes of Chondritic Components. *Rev. Mineral. Geochem.* **68**, 141–186.

TABLE 1

Table 1: Average mineral chemistry and host oxygen isotope ratios (‰, VSMOW) of individual chondrules in the polished thin section of Kaba CV3 (USNM 1052-1).

Chondrule	Type	Ol-r[a]	Ol-h[a]	Px[a]	Mg#[b]	Wo[c]	$\delta^{18}O$[d]		$\delta^{17}O$[d]		$\Delta^{17}O$[d]	
K1 (core)	IAB	-	12	9	99.0	1	−1.79	±0.33	−5.15	±0.24	−4.22	±0.17
K1 (rim)	-	-	-	2	98.4	1	−1.79	±1.36	−4.91	±0.72	−3.98	±0.29
K1 (all)	IAB	-	12	11	98.8	1	−1.79	±0.34	−5.13	±0.24	−4.20	±0.17
K2	IA	2	6	2	99.2	2 (1-2)	−3.07	±0.50	−6.05	±0.32	−4.45	±0.29
K3	IAB	-	4	4	99.3	1	−2.12	±0.42	−5.00	±0.24	−3.89	±0.26
K4	IA	6	1	2	99.5	1	−6.91	±0.49	−9.66	±0.44	−6.07	±0.28
K5	IAB	3	-	5	99.3	3 (1-5)	−4.46	±0.47	−7.87	±0.45	−5.56	±0.28
K6	IA	-	6	4	99.3	3 (1-3)	−2.45	±0.44	−5.66	±0.37	−4.39	±0.21
K7	IA	-	5	3	99.4	1	−5.45	±0.40	−8.11	±0.22	−5.28	±0.16
K8	IAB	-	6	4	99.3	1	−5.75	±0.40	−8.78	±0.31	−5.79	±0.19
K9	IAB	-	2	3	99.4	2 (1-5)	−5.34	±0.86	−8.30	±0.65	−5.53	±0.27
K8+9 (rim)	-	-	-	4	99.1	4 (1-5)	−4.47	±0.36	−7.61	±0.30	−5.28	±0.23
K8+9 (all)	IAB	-	8	11	99.3	2 (1-5)	−5.37	±0.46	−8.41	±0.36	−5.62	±0.19
K10	IA	1	4	5	99.0	4 (4-5)	−2.67	±0.37	−5.77	±0.29	−4.38	±0.19
K11	IB	-	3	4	99.2	1 (1-3)	−3.16	±0.39	−6.33	±0.26	−4.68	±0.19
K12	IAB	1	3	5	99.1	1 (1-2)	−4.73	±0.37	−7.85	±0.26	−5.39	±0.18
K13	IB	3	-	5	99.0	2 (1-4)	−3.08	±0.49	−6.09	±0.29	−4.48	±0.23
K14	IAB	1	3	4	99.1	1	−4.31	±0.39	−7.64	±0.29	−5.40	±0.24
K15	IB	-	4	4	99.4	1	−5.85	±0.41	−8.87	±0.25	−5.83	±0.18
K16	IA	6	-	4	99.2	5	−4.62	±0.42	−7.43	±0.29	−5.03	±0.27
K17	IAB	-	5	3	99.4	1	−4.90	±0.36	−7.94	±0.26	−5.40	±0.21
K18	IA	3	3	1	99.6	1	−11.96	±0.41	−14.48	±0.28	−8.26	±0.14
K19	IAB	-	5	2	99.3	1	−4.37	±0.65	−7.56	±0.42	−5.29	±0.18
K20	IAB	2	3	2	99.2	1	−4.10	±0.75	−7.41	±0.61	−5.28	±0.26
K21	IAB	-	5	3	99.2	1	−3.41	±0.34	−6.97	±0.30	−5.20	±0.26
K22	IAB	-	4	4	98.8	1	−2.74	±0.53	−5.79	±0.38	−4.37	±0.26
K23	IAB	-	4	-	99.5	-	−7.02	±0.31	−11.44	±0.40	−7.79	±0.37
K24	IAB	1	3	4	99.4	1	−5.29	±0.69	−8.48	±0.63	−5.73	±0.36
K25	IIB	-	-	3	85.7	1	3.82	±0.35	2.04	±0.30	0.06	±0.24
K26	IIA	-	4	-	62.9[e]	-	2.74	±0.34	−0.80	±0.38	−2.22	±0.28

[a] Ol-r, Ol-h, and Px represent the number of SIMS analyses from relict olivine, host olivine, and low-Ca pyroxene, respectively. [b] Mean Mg# (MgO/(MgO+FeO) mol%) of olivine and pyroxene excluding relict olivine. [c] Mean Wo component of low-Ca pyroxenes in mol%; ranges shown in parenthesis, if significantly variable. [d] Quoted

uncertainties are at 95% confidence level. Analyses of relict olivine are not included in the mean values.[e] Olivine zoned in Mg# (core ~58, rim ~66).

FIGURE CAPTIONS

Figure 1: Representative BSE images of chondrules from the Kaba USNM 1052-1 thin section showing SIMS pits for oxygen three-isotope analyses (except for K1). (a) compound chondrule K8+9 (IAB) enclosed in igneous rim comprising pyroxene, olivine and opaque phases. (b) K1 (IAB) composed of coarse-grained olivine and pyroxene phenocrysts, as well as anorthite and high-Ca pyroxene in mesostasis at the chondrule center; enclosed in relatively fine-grained and opaque phases-rich rim. (c) K22 (IAB) contains coarse-grained olivine and low-Ca pyroxene. Altered mesostasis comprises phyllosilicates and high-Ca pyroxenes, latter forming euhedral overgrowths on low-Ca pyroxenes. (d) low-Ca pyroxene poikilically encloses olivine in K11 (IB). (e) K16 (IA) comprises small amount of mesostasis and intermediate pyroxene alongside olivine. (f) FeO-rich low-Ca pyroxenes (En85) in K25 (IIB) possess overgrowth of FeO-rich olivine (Fo83). Ol: olivine, Lpx: low-Ca pyroxene, HPx: high-Ca pyroxene, IntPx: intermediate pyroxene, An: anorthite, Phy: phyllosilicates; scale in all images: 500μm.

Figure 2: Oxygen three-isotope diagram showing olivine (n=124) and pyroxene (n=95) analyses from chondrules in Kaba. Most analyses plot on the primitive chondrule mineral (PCM; Ushikubo et al., 2012) line or in between the PCM and CCAM (Clayton et al., 1977) lines; analyses of chondrule K25 plot above PCM and on terrestrial fractionation (TF) line. YR: Young & Russel line (Young and Russell, 1998).

Figure 3: Oxygen three-isotope diagrams of individual olivine and pyroxene analyses of representative chondrules in Kaba. Error bars show external reproducibility (2SD) obtained by analyses of the bracketing olivine standard. (a-g) Individual analyses are indistinguishable in

terms of their $\Delta^{17}O$ values within the variability threshold of ±0.6‰. (h) One olivine analysis in chondrule K14 slightly exceeds variability threshold. (i-j) Olivine and pyroxene analyses form distinct clusters, while (relict) olivine are either ^{16}O-rich (K13) or ^{16}O-poor (K16) relative to pyroxene. (k-l) analyses of K6 and K8+9 show clearly resolvable variability in $\delta^{18}O$ and $\delta^{17}O$ values (2SD: 1.0‰ – 1.4‰) but $\Delta^{17}O$ values are within variability threshold (±0.6‰). Both chondrules are marginally heterogeneous. In K6 (k), analyses located in right hand part of chondrule are relatively more ^{16}O-rich (circled data points). In K8+9 (l) pyroxene analyses in the rim and a few locations of the chondrule interior (circled data points) are ^{16}O-poor relative to the rest of the analyses.

Figure 4: $\Delta^{17}O$ values of olivine and pyroxene analyses per individual chondrule. Error bars show external reproducibility (2SD) obtained by analyses of the bracketing standard. Chondrules sorted according to increasing host chondrule $\Delta^{17}O$ values (stars) which are obtained by averaging $\Delta^{17}O$ values of isotopically homogeneous olivine and/or pyroxene analyses after excluding isotopic relicts (triangles). $\Delta^{17}O$ values of relict olivine exceed the variability threshold (grey line; ±0.6‰, mean external precision on bracketing standard, 3SD). Most type I chondrules show host chondrule $\Delta^{17}O$ values in between –6‰ and –4‰ as illustrated by the histogram on the right-hand side of the graph.

Figure 5: Mean olivine and pyroxene (a) $\Delta^{17}O$ and (b) $\delta^{18}O$ values of individual chondrules. (a) Chondrule means ($\Delta^{17}O$) of olivine and pyroxene (excluding relict olivine) are shown for chondrules that have indistinguishable olivine and pyroxene analyses. Error bars show the propagated uncertainties of the mean values (see Section 2.4. and Tab. 1). (b) Mean olivine $\delta^{18}O$ values are slightly higher than those of pyroxene but variations are within propagated uncertainties.

Figure 6: Host chondrule isotope ratios ($\delta^{18}O$, $\delta^{17}O$, and $\Delta^{17}O$) and textures of chondrules. Error bars represent propagated uncertainty of the mean values. (a) Oxygen 3-isotope diagram showing chondrule means. Reference lines are the same as those in Fig. 2. Host values of chondrules plot on the PCM line or slightly below. Exceptions are chondrules K23 (IAB) and K25 (IIB). (b) Host $\Delta^{17}O$ values are independent of chondrule texture among type I chondrules. Type II chondrules are ^{16}O-poor compared to type I chondrules.

Figure 7: Plot showing host $\Delta^{17}O$ values and Mg#'s of chondrules superimposed by oxygen isotope mixing curves of constant dust enrichment and ice enhancement from the model of Tenner et al. (2015). The model adopts the following $\Delta^{17}O$ values for the various oxygen reservoirs: anhydrous silicate dust, –8.0‰; Solar gas, –28.4‰; water ice, +2.0‰; organics in the dust, +11.3‰. Inferred anhydrous dust enrichment and ice enhancement factors for type I chondrules are 50-100× relative to Solar abundance and from anhydrous to ~0.6× the water ice content of dust of CI composition, respectively. Mg#'s and $\Delta^{17}O$ values of the type II chondrules suggest higher : (IIB: ~300×, IIA: ~2000×) dust enrichment factors and water ice contents (1-4× the amount of water ice of dust of CI composition). The error bars for Mg#'s represent the range (min-max); for host (mean) $\Delta^{17}O$ values, error bars are propagated uncertainties (see Tab. 1).

Figure 8: Histograms of host $\Delta^{17}O$ values from chondrules in Kaba and further carbonaceous chondrites. Like Kaba, all listed carbonaceous chondrites contain abundant type I chondrules with $\Delta^{17}O$ values in the range of ~ –6‰ and –4‰, though no type I chondrules in Kaba show $\Delta^{17}O$ values > –3‰ that are common in the other carbonaceous chondrites except Yamato 82094. Because Allende experienced significant thermal metamorphism, Mg#'s of chondrules are disturbed and no distinction is being made between type I chondrules with Mg#<98 or >98.

Literature data are from [1] Rudraswami et al. (2011), [2] Tenner et al. (2013), [3] Tenner et al. (2015), [4] Tenner et al. (2017), [5] Ushikubo et al. (2012).

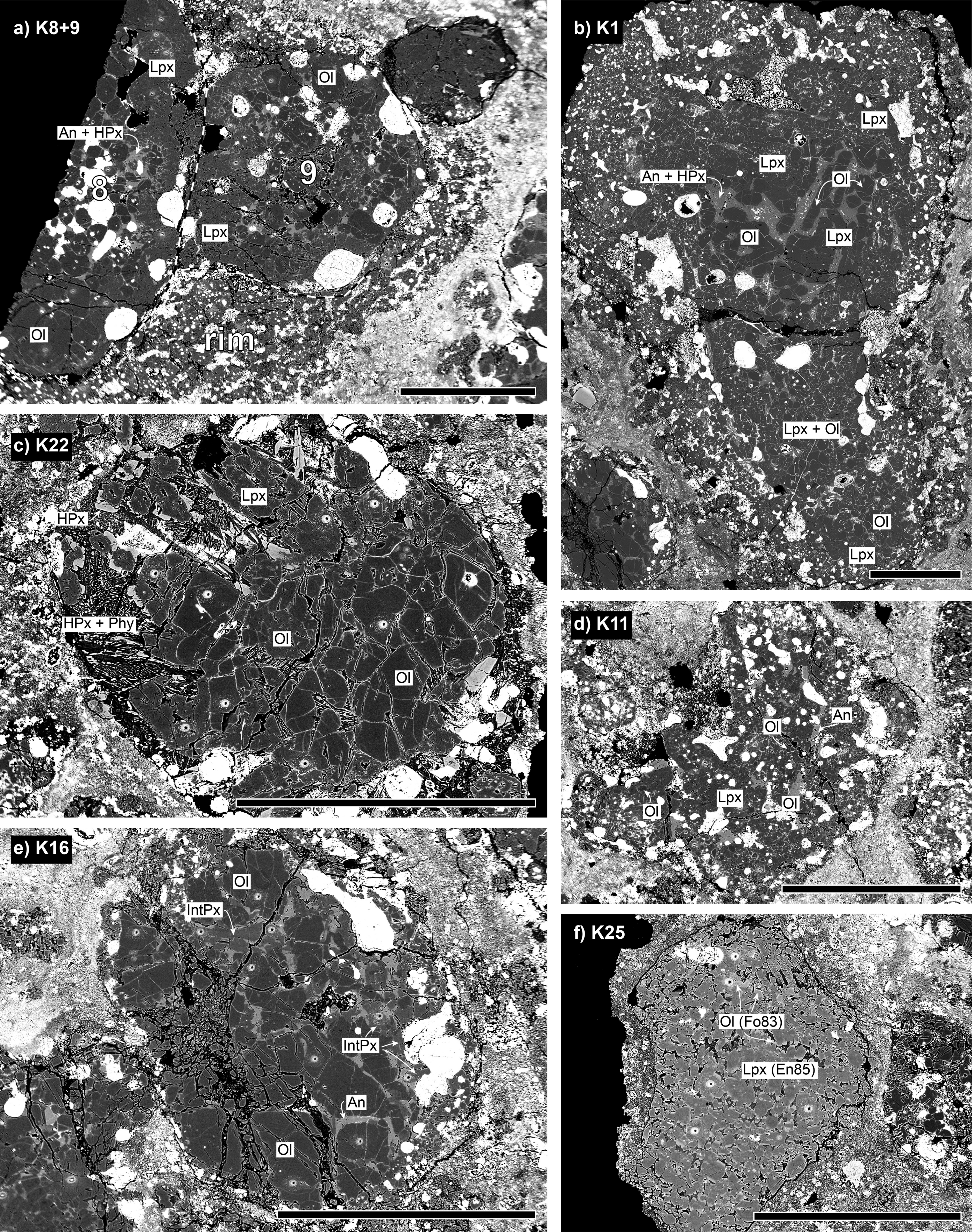
a) K8+9
Lpx
An + HPx
8
9
Ol
Lpx
Ol
rim
b) K1
Lpx
Lpx
An + HPx
Ol
Ol
Lpx
Lpx + Ol
Ol
Lpx
c) K22
Lpx
HPx
HPx + Phy
Ol
Ol
d) K11
An
Ol
Lpx
Ol
Ol
e) K16
Ol
IntPx
IntPx
An
Ol
f) K25
Ol (Fo83)
Lpx (En85)

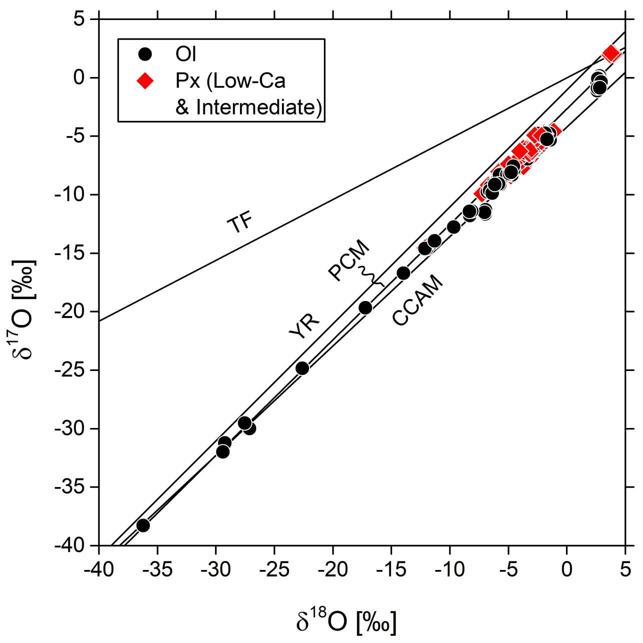

Ol
Px (Low-Ca
& Intermediate)
TF
PCM
YR
CCAM
δ^{17}O [‰]
δ^{18}O [‰]
5
0
-5
-10
-15
-20
-25
-30
-35
-40
-40
-35
-30
-25
-20
-15
-10
-5
0
5

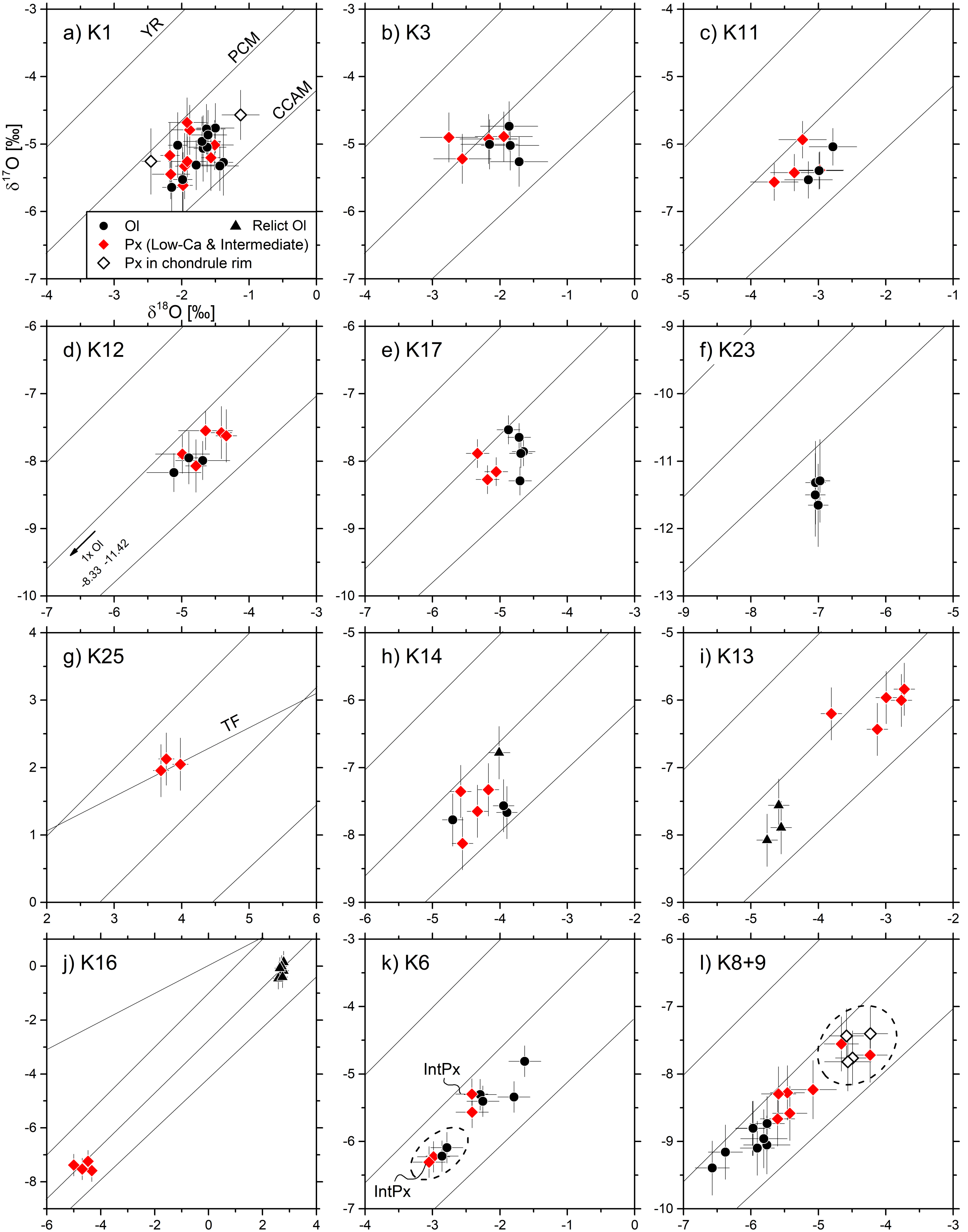

a) K1
YR
PCM
CCAM
δ17O [‰]
δ18O [‰]
Ol
Relict Ol
Px (Low-Ca & Intermediate)
Px in chondrule rim
b) K3
c) K11
d) K12
1x Ol
-8.33 -11.42
e) K17
f) K23
g) K25
TF
h) K14
i) K13
j) K16
k) K6
IntPx
IntPx
l) K8+9

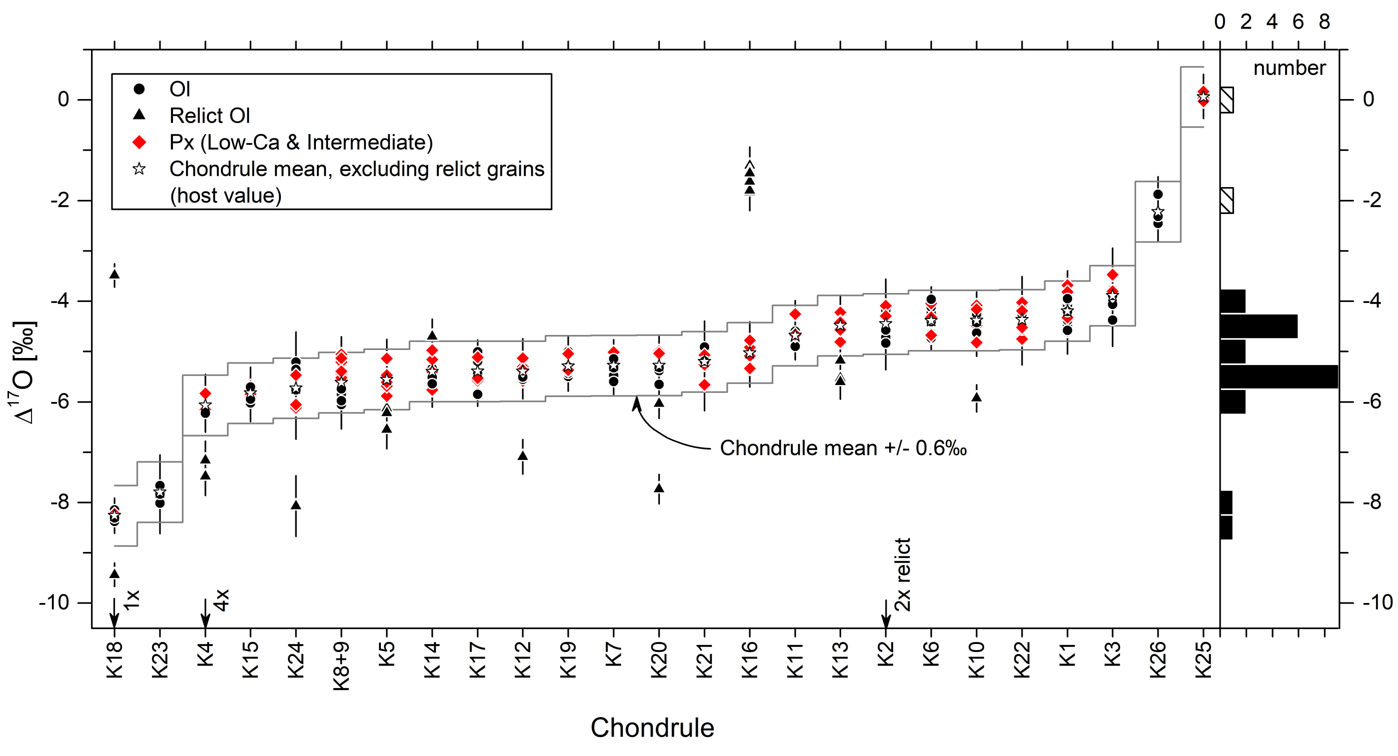

Ol
Relict Ol
Px (Low-Ca & Intermediate)
Chondrule mean, excluding relict grains
(host value)
Δ17O [‰]
Chondrule
number
Chondrule mean +/- 0.6‰
1x
4x
2x relict
K18
K23
K4
K15
K24
K8+9
K5
K14
K17
K12
K19
K7
K20
K21
K16
K11
K13
K2
K6
K10
K22
K1
K3
K26
K25
0
-2
-4
-6
-8
-10
0 2 4 6 8

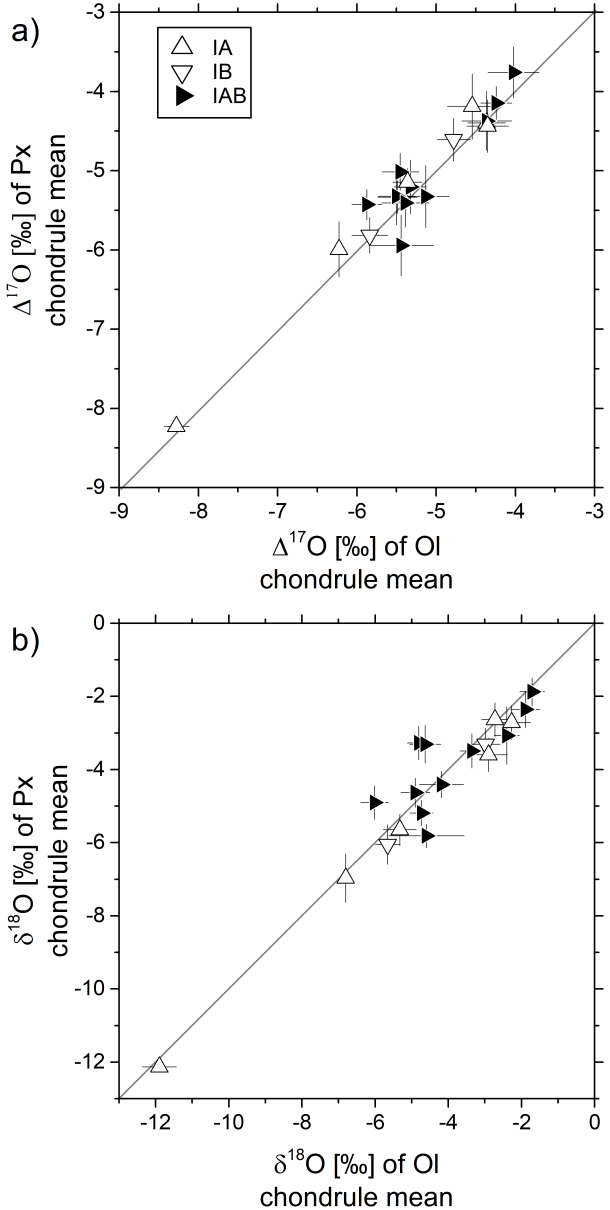
a)
IA
IB
IAB
Δ17O [‰] of Px chondrule mean
Δ17O [‰] of Ol chondrule mean
-3
-4
-5
-6
-7
-8
-9
b)
δ18O [‰] of Px chondrule mean
δ18O [‰] of Ol chondrule mean
0
-2
-4
-6
-8
-10
-12

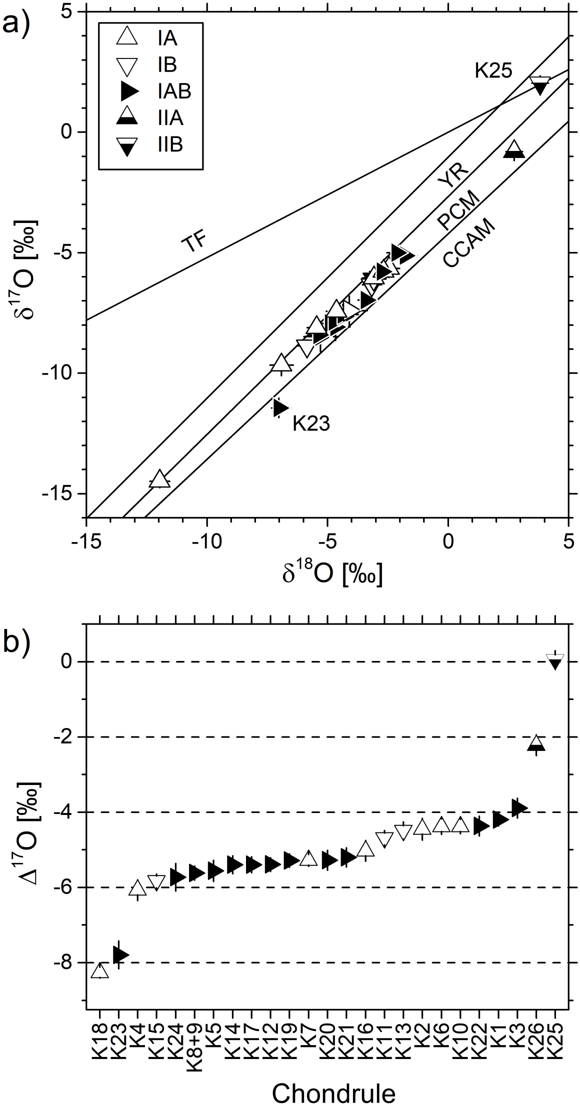

a)
IA
IB
IAB
IIA
IIB
K25
TF
YR
PCM
CCAM
K23
δ17O [‰]
δ18O [‰]
b)
Δ17O [‰]
K18
K23
K4
K15
K24
K8+9
K5
K14
K17
K12
K19
K7
K20
K21
K16
K11
K13
K2
K6
K10
K22
K1
K3
K26
K25
Chondrule

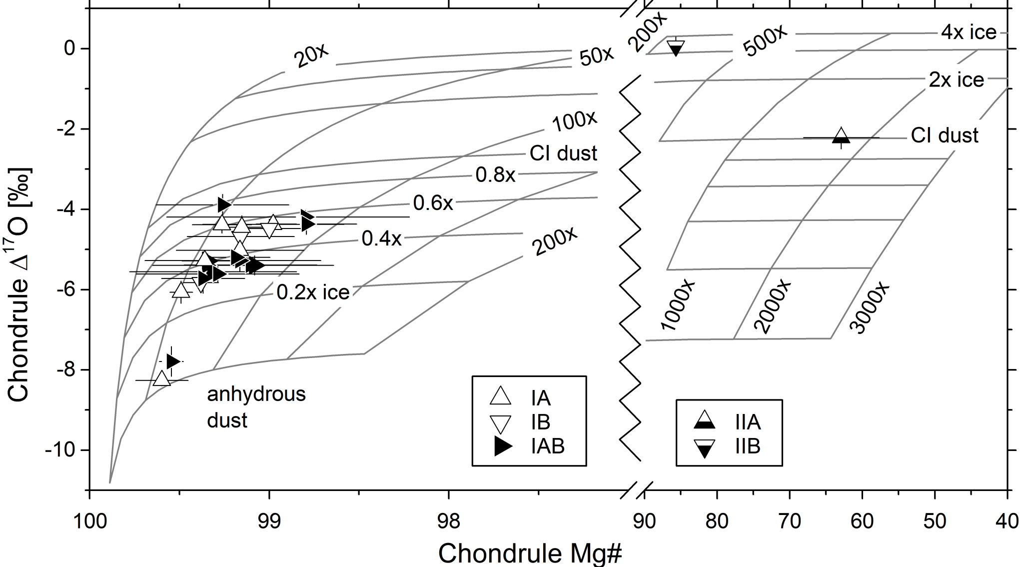

Chondrule Δ¹⁷O [‰]
Chondrule Mg#
0
-2
-4
-6
-8
-10
100
99
98
90
80
70
60
50
40
20x
50x
100x
CI dust
0.8x
0.6x
0.4x
0.2x ice
200x
anhydrous
dust
200x
500x
4x ice
2x ice
CI dust
1000x
2000x
3000x
IA
IB
IAB
IIA
IIB

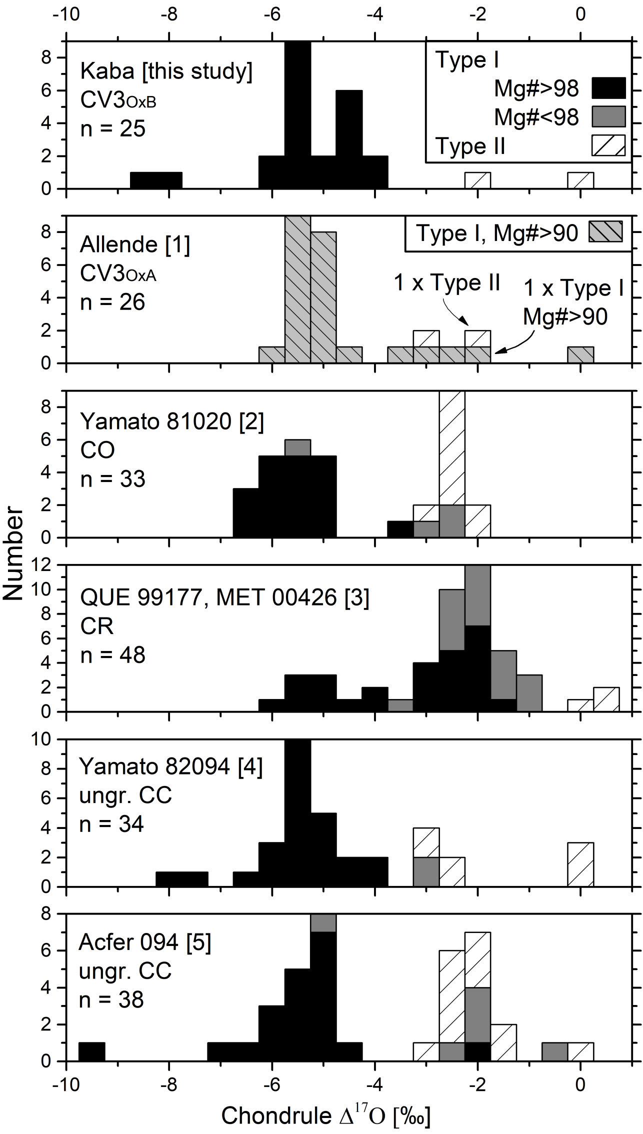

Kaba [this study]
CV3OxB
n = 25
Type I
Mg#>98
Mg#<98
Type II
Allende [1]
CV3OxA
n = 26
Type I, Mg#>90
1 x Type II
1 x Type I
Mg#>90
Yamato 81020 [2]
CO
n = 33
QUE 99177, MET 00426 [3]
CR
n = 48
Yamato 82094 [4]
ungr. CC
n = 34
Acfer 094 [5]
ungr. CC
n = 38
Number
Chondrule Δ17O [‰]